Aerosol and Air Quality Research, 16: 2396–2404, 2016

ISSN: 1680-8584 print / 2071-1409 online
doi: 10.4209/aaqr.2015.09.0554

Vertical Circulation of Atmospheric Pollutants near Mountains during a Southern California Ozone Episode

Hiroaki Minoura[1*†], Judith C. Chow[2], John G. Watson[2], Joshua S. Fu[3], Xinyi Dong[3], Cheng-En Yang[3]

[1] *Toyota Central R&D Labs. Inc., Nagakute, Aichi 480-1192, Japan*
[2] *Division of Atmospheric Science, Desert Research Institute, Reno, NV 89512, USA*
[3] *Department of Civil and Environmental Engineering, University of Tennessee, Knoxville, TN 37996, USA*

ABSTRACT

This study investigates the air pollutant interactions and emission source contributions to ozone (O_3) formation within a complex terrain. Air quality simulations using the Community Multiscale Air Quality (CMAQ) Model focused on vertical distributions of O_3 for the July 14–18, 2005 episode in the South Coast Air Basin (SoCAB). The Zero-Out method was applied in sensitivity tests for seven emission source categories. Elevated O_3 concentrations were found near the top of the planetary boundary layer (PBL, ~1200 m) and in the free troposphere (~3500 m) over the eastern SoCAB. Low O_3 concentrations were found near the surface at the center of the basin due to nitrogen oxide (NO) titration by fresh vehicle exhaust. Sea and land breezes, enhanced by up-slope flows (the "mountain chimney effect") transported O_3 upward. Formation of O_3 is sensitive to the H_2O_2/HNO_3 ratio, depending on fresh vs. aged pollutant mixtures. Biogenic emissions were important contributors to O_3 formation, both in the SoCAB and at the top of the PBL. In contrast, the highest vehicle contributions to O_3 were found far from urban areas and in the lower free troposphere. Vertical cross-sectional analysis provided some insights into the O_3 formation and mixing processes present in the SoCAB.

Keywords: Ozone formation; Source contribution; Vertical circulation; Model simulation.

INTRODUCTION

The South Coast Air Basin (SoCAB) in California, including the city of Los Angeles (LA), is located in complex terrain surrounded by mountains with ridges of more than 2000 m above mean sea level (asl). Anthropogenic air pollutants from urban areas, transported by sea breezes, contribute to high ozone (O_3) concentrations on the mountain slopes of the eastern SoCAB during summer.

Insufficient ventilation and accumulation of photochemical air pollutants in the SoCAB have been studied since Haagen-Smit (1952). The area has been known to report the highest O_3 concentrations in the U.S. Hourly O_3 concentrations, which exceeded 500 ppb during the 1960s, have been reduced to < 120 ppb for the maximum 8-hr average in recent years. Fujita *et al.* (2013) showed the decreasing O_3 trend in SoCAB, and pointed to changes in the photochemical reaction due to variations in volatile organic compound (VOC)/oxides of nitrogen (NO_x) ratios during the past three decades.

Updrafts generated by solar radiation on mountain slopes result in vertical transport of air pollutants, called the "mountain chimney effect", (e.g., Lu and Turco, 1996; Langford *et al.*, 2010). Three-dimensional (3-D) observations using aircraft and remote sensors, such as NASA's Discover-AQ (http://www.nasa.gov/mission_pages/discover-aq/news/DAQ-20130226.html) have improved understanding of the vertical structure of these events. To understand air pollutant evolution in complex terrain, it is important to consider O_3 formation through atmospheric transport and photochemical reactions of pollutants.

Since three-dimensional observations have temporal and spatial limitations, a comprehensive chemistry-transport model can be a useful complement to understand the influence of transport and chemical mechanisms. Most air quality modelling efforts have estimated present and future ground-level concentrations, with little attention given to O_3 that accumulates aloft, especially near mountainous terrain. Only a few of these studies examined the source-specific contributions to high O_3 levels.

Zhang *et al.* (2014) examined emission source contributions

† Now at Asia Center for Air Pollution Research, 1182 Sowa Nishi-ku, Niigata-shi, 950-2144, Japan

* Corresponding author.
Tel.: 81-24-263-0557; Fax: 81-25-263-0567
E-mail address: minoura@acap.asia

to fine particles and O_3 concentrations for eight large cities in the southeastern U.S. With respect to engine exhaust contributions to O_3 formation, NO_x titration yielded negative effects within the urban centers, overall contributions were low for nearby suburban ground-based concentrations, but exhaust contributions to O_3 increased 30–50 km far from the city centers, especially in mountainous regions. Similar results were observed by Collet *et al.* (2012), with SoCAB O_3 concentrations downwind of the urban center being influenced by engine exhaust. However, it is difficult to determine which types of emissions have the greatest impact on O_3 formation given the complex interactions among emissions, meteorology, and photochemistry in complex terrain.

In this study, a high SoCAB O_3 episode near the San Bernardino Mountains in the eastern part of the basin is investigated with the Community Multiscale Air Quality (CMAQ) Modeling System (Byun and Schere, 2006). Instead of examining the horizontal distribution for ground-based concentration, the approach taken here details vertical transects while systematically eliminating precursor emissions from major SoCAB source categories. Ratios of precursor, intermediate and end-product concentrations, which are also calculated by CMAQ, are used to better understand the atmospheric chemistry.

METHODS

Table 1 summarizes the simulation conditions and model configuration. Emission inputs were obtained from the U.S. EPA 2005 National Emissions Inventory (NEI) processed by the Sparse Matrix Operator Kernel Emissions (SMOKE) Model (Version 3.0). Meteorological fields were provided by the Weather Research & Forecasting (WRF) Model (Version 3.3), and air quality simulations were conducted using CMAQ Version 4.7.1. The modeling domain (912 km west/east × 672 km north/south) consisted of 229 × 169 horizontal grids with a horizontal resolution of 4 km. This domain includes the Pacific Ocean to the west (Longitude -122.485 degrees; 376 km from the coast), the cities of LA and Riverside, the city of Santa Barbara to the northwest, with the San Bernardino Mountain (SB-Mtn) range to the east. The surface layer thickness was 12.3 m. The model vertical extent up to a maximum height of 20656 m above sea-level (asl) was discretized with 41 layers. The CMAQ and WRF domains and grid sizes were the same. A five-day O_3 episode started at 0000 (GMT) July 14), 2005, with a spin-up period of ~21 hours. O_3 formed after spin-up (i.e., after ~1300 (PST) on July 14) is discussed here. The initial concentrations and boundary concentrations used CMAQ default values (e.g. boundary ozone concentration at sea surface, land surface, and atmospheric top was 35 ppb, 30 ppb, and 70 ppb, respectively).

One-hour average O_3 concentration for 96 hours measured at 43 monitoring sites of the U.S. EPA in SoCAB were compared with CMAQ simulation results of the relevant time period and location in Table 2; the mean normalized bias (MNB), the mean normalized gross error (MNGE), and the peak accuracy ratio of 9.5, 15.4, and 16.3%, respectively, show reasonably good agreement. Large discrepancies were found at three monitoring sites located near the northwest computational domain near Bakersfield. However, obtained MNB and MNGE result in significantly less than 15 and 30%, respectively, which is the former simulation guideline of U.S. EPS. In addition, correlation between O_3 concentration measured at the San Bernardino-4th Street site and the Pomona site close to the point shown Fig. 1(b), were both 0.86, and further discussion with this accuracy is considered to be possible.

Several methods have been used to evaluate source contributions to O_3, such as sensitivity analysis using the decoupled direct method (DDM) (Dunker, 1984), the source oriented tagged methods: OSAT (Ozone Source Apportionment Technology; Yarwood *et al.*, 1997), or the Integrated Source Apportionment Method (ISAM; Release notes for CMAQ Version 5.0.2). The brute force method (BFM), a sensitivity analysis tool, is applied for this study with 100% emission reductions (i.e., Zero-Out method) for seven major source types, including: on-road gasoline engine exhaust, on-road diesel engine exhaust, non-road gasoline engine exhaust, non-road diesel engine exhaust, industrial (including point sources, i.e., power plant, boilers, steel industry, and solvent utilization), residential, and biogenic emitters. Area source emissions from small factories, offices, and homes are included in the residential category, whereas wildfires are included with biogenic emissions.

Table 1. Summary of CMAQ model simulation conditions for the period of July 14–18, 2005 (GMT).

Input Parameter	Model/Data Source
Base emission	U.S. EPA 2005 National Emissions Inventory (NEI)
Emission model	SMOKE (Version 3.0)
Meteorological model	WRF (Version 3.3)
Air quality model	CMAQ (Version 4.7.1)
Horizontal grid	229 × 169 grid at 4 km
Vertical layer	41 layers up to 20,643 m
Chemical model	CB05CL_AE5_AQ
Horizontal advection	Global mass-conserving (Yamartino) scheme
Vertical advection	Global mass-conserving scheme
Horizontal diffusion	Diffusion coefficient based on local wind
Vertical diffusion	Asymmetric Convective Model (Version 2)
Boundary & initial concentrations	CMAQ default values

Table 2. Comparison between model simulation and ambient measurements.

Parameter	Equation	Results
Mean Normalized Bias (MNB)	$MNB = \frac{1}{N}\sum_{i=1}^{N}\frac{M_i - O_i}{O_i}$	9.5%
Mean Normalized Gross Error (MNGE)	$MNGE = \frac{1}{N}\sum_{i=1}^{N}\frac{\lvert M_i - O_i\rvert}{O_i}$	15.4%
Peak Accuracy (PA) ratio	$PA = \left(\frac{MNB}{MNGE}\right)_{max\ conc.}$	16.3%

aM_i = Model concentration for species i.
O_i = Observed concentration for species i.

Vertical wind velocities were estimated from the convergence and divergence of horizontal wind velocities in CMAQ-ready wind data for hydrostatic balance. The basic equations and methods follow those of Kato and Saito (1995). To explore a refined 3-D distribution of air pollutants and air flows, data visualization with Cartesian coordinates instead of spatial plots with σP coordinates (the original system in the CMAQ Model) are used. (The σP coordinate system is a common coordinate system used in computational models, the details numerical handling is described in Zavisa Janjic *et al.*, 2010.)

RESULTS

Fig. 1 shows an example of vertical O_3 and wind distributions. For better resolution, finer vertical coordinate grids of CMAQ are used at the altitude close to the surface according to the vertical coordinate parameter (VGLVLS). Fig. 1(a) includes the direct CMAQ output. The vertical spacing differs for sea and mountain because the simulation is conducted in σP coordinates. Fig. 1(b) was obtained by converting the Fig. 1(a) data to Cartesian coordinates relative to mean sea level. As a result of this conversion, the relationships among the terrain, vertical convection, and O_3 concentrations are better illustrated. The influence of stratospheric O_3 on tropospheric O_3 at < 5000 m asl is negligible small.

At 1800 PST on July 17, O_3 concentrations were lowest (below 453 m asl) in the LA area, consistent with NO titration by evening traffic. Elevated O_3 concentrations (> 75 ppb) were found at the top of the planetary boundary layer (PBL, ~1200 m asl), near the ridgelines of the San Bernardino Mountain Range (1518 m at San Gorgonio Mountain), and in the free troposphere (~3500 m asl). This finding is similar to those reported by Lu and Turco (1996) using the Surface Meteorology and Ozone Generation (SMOG) Model. The presence of elevated O_3 concentrations at ~4000 m was also identified from airborne Lidar measurements (Langford *et al.* (2010)). Counter-clockwise air flow and pollutant circulation was found on the western

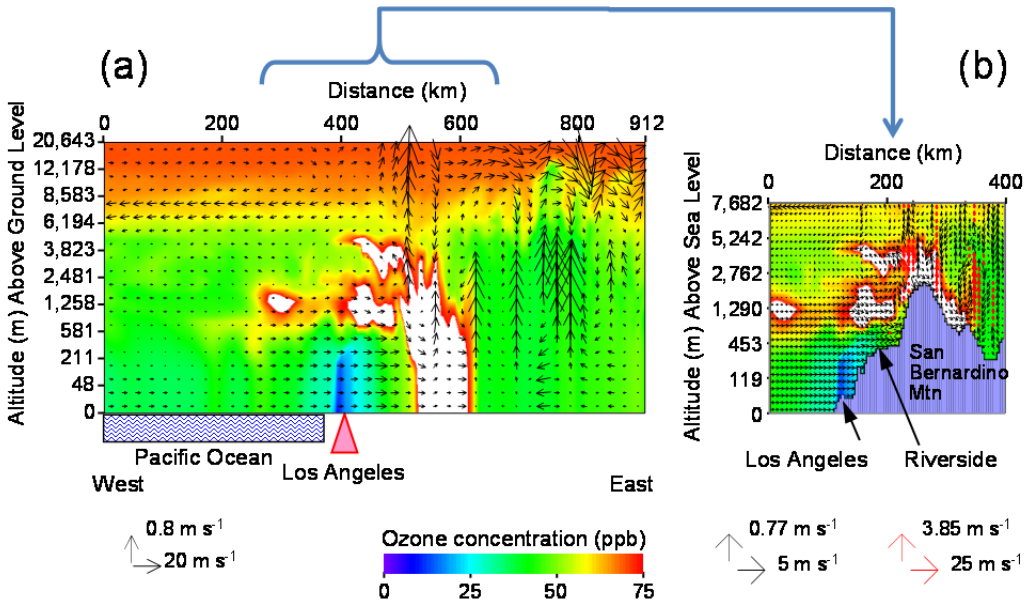

Fig. 1. July 17, 2005, 1800 PST (a) vertical O_3 cross-section and winds with elevations derived from σP used in CMAQ; and (b) a magnification of a with vertical elevations translated to linear Cartesian coordinates. O_3 concentrations > 75 ppb are shown in white. Wind speed is indicated by arrow with different scales in the horizontal and vertical direction.

and eastern sides of San Bernardino range. These types of vortices were most prominent during early evening. Elevated O_3 concentrations in the free troposphere were likely transported by the updraft flow (i.e., the mountain chimney effect). Up-slope flows and high O_3 concentrations were also found on July 14. O_3 concentrations were > 75 ppb near the top of the PBL and vertical convection was found on all five days (July 14–18) of the simulation.

High O_3 concentrations at the top of the PBL over the Pacific Ocean in middle left part of Fig. 1(b) most likely resulted from aged air transported from the northwest. Using a Lagrangian simulation, Angevine *et al.* (2013) showed that a mixture of aged carbon monoxide (CO) can be transported from the Bay Area in Northern California to Southern California. This is caused by the prevailing northwesterly winds down the coast and circulated by the "Catalina Eddy" (Angevine *et al.*, 2012). High O_3 concentrations above the PBL and over the San Bernardino range in Fig. 1(b) were likely generated from fresh air pollutants from the urban areas between the cities of LA and Riverside.

Horizontal O_3 distributions near the top of the PBL (1179 m asl, Fig. 2(a)) differed from those in the free troposphere (3417 m asl, Fig. 2(b)). O_3 near the top of PBL, shown in Fig. 2(a), was a mixture of O_3 formed at the mountainside of the San Bernardino Mountain Range and O_3 transported from the northwest. The trajectory of Fig. 2(a) shows that the high O_3 originated from the direction of Santa Barbara (~150 km northwest of the SoCAB). The centroid of the high O_3 cloud moved along the advection current to the southeast, and diminished around midnight. In contrast, smaller temporal and spatial variations in O_3 were found in the free troposphere. Fig. 2(b) (~1800 PST) also identifies hot spots (shown in white) during the day. Re-circulation in higher altitude, as opposed to advection of lower level shown in Fig. 2(a), is consistent with the transport of locally generated air pollutants in the SoCAB.

Fig. 3 shows the vertical distribution of precursor gases that correspond to the vertical O_3 distribution in Fig. 1(b). Since large amounts of nitric oxide (NO) due to human activities are released into the atmosphere, a high concentration was seen in LA as shown in Fig. 3(a). As marine-transported O_3 mixed and reacted with NO in LA, O_3 concentrations decreased, consistent with high NO and nitrogen dioxide (NO_2) concentrations in the western part of the basin, and as shown in Fig. 3(b), high NO_2 concentrations in the western and eastern parts of the SoCAB which was transported eastward by the sea breeze. The highest NO_2 concentration was found over the western mountain slopes. A wider and deeper distribution was found for VOCs as shown in Fig. 3(c), as up-slope flows transported VOCs above the PBL. Elevated VOCs over the Pacific Ocean at the top of PBL may reflect VOC transport from the northwest. Fig. 3(d) shows nitric acid (HNO_3) concentrations resulting from NO_x oxidation. HNO_3 concentrations were highest downwind (eastward) of high NO_x concentrations, consistent with elevated NO (i.e., fresh vehicle exhaust emission) in the western part of the SoCAB. Higher HNO_3 concentrations were found above the PBL, possibly resulting from vertical mixing. High hydrogen peroxide (H_2O_2) concentrations at the top of the PBL over the Pacific Ocean (Fig. 3(e)), similar to those found for VOC in Fig. 3(c), were apparently affected by transport from the northwest.

H_2O_2 to HNO_3 ratios have been used as chemical indicators for O_3 formation (Sillman, 1995; Tonnesen and Dennis, 2000a, b; Sillman and He, 2002). Hydroxyl radicals (OH), which are photolysis-generated radicals from O_3 to olefin reaction, and aldehyde produce H_2O_2 via hydroperoxide (HO_2). HO_2 radicals and OH also produce HNO_3 from NO via NO_2. Since HNO_3 is to be generated earlier than H_2O_2 in the photolysis process and shows a tendency to decrease at night, H_2O_2/HNO_3 ratios also serve as an indicator of aging. The H_2O_2/HNO_3 ratio shows

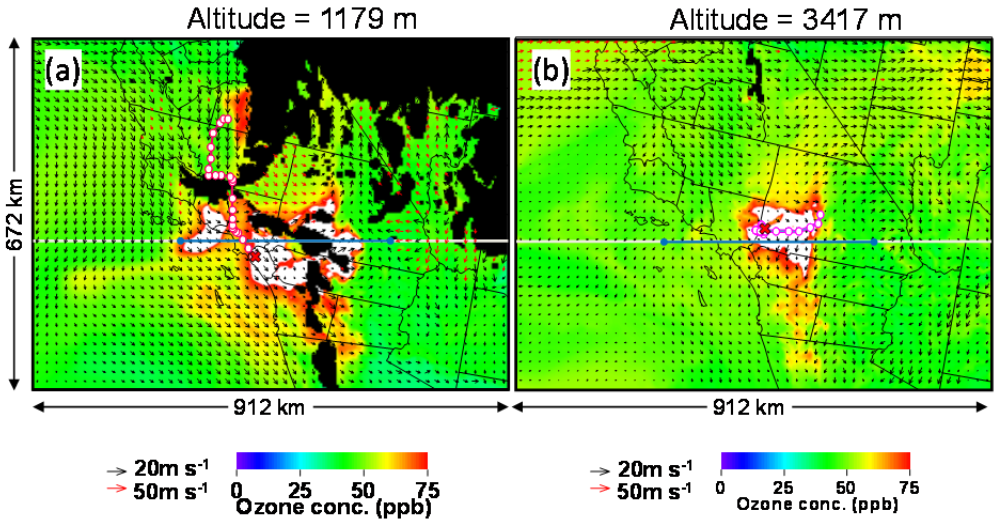

Fig. 2. Horizontal O_3 concentrations and wind fields at 1800 PST on July 17, 2005 at: (a) 1179 m asl (closest to the top of the planetary boundary layer [PBL]), and (b) 3417 m asl (in the free troposphere). Black areas indicate locations of mountains. The blue bar shows the area corresponding to the latitude cross-section in Fig. 1(b). Pink circles indicate one-hour back-trajectory segments from the point of highest O_3 concentration of a red-cross symbol.

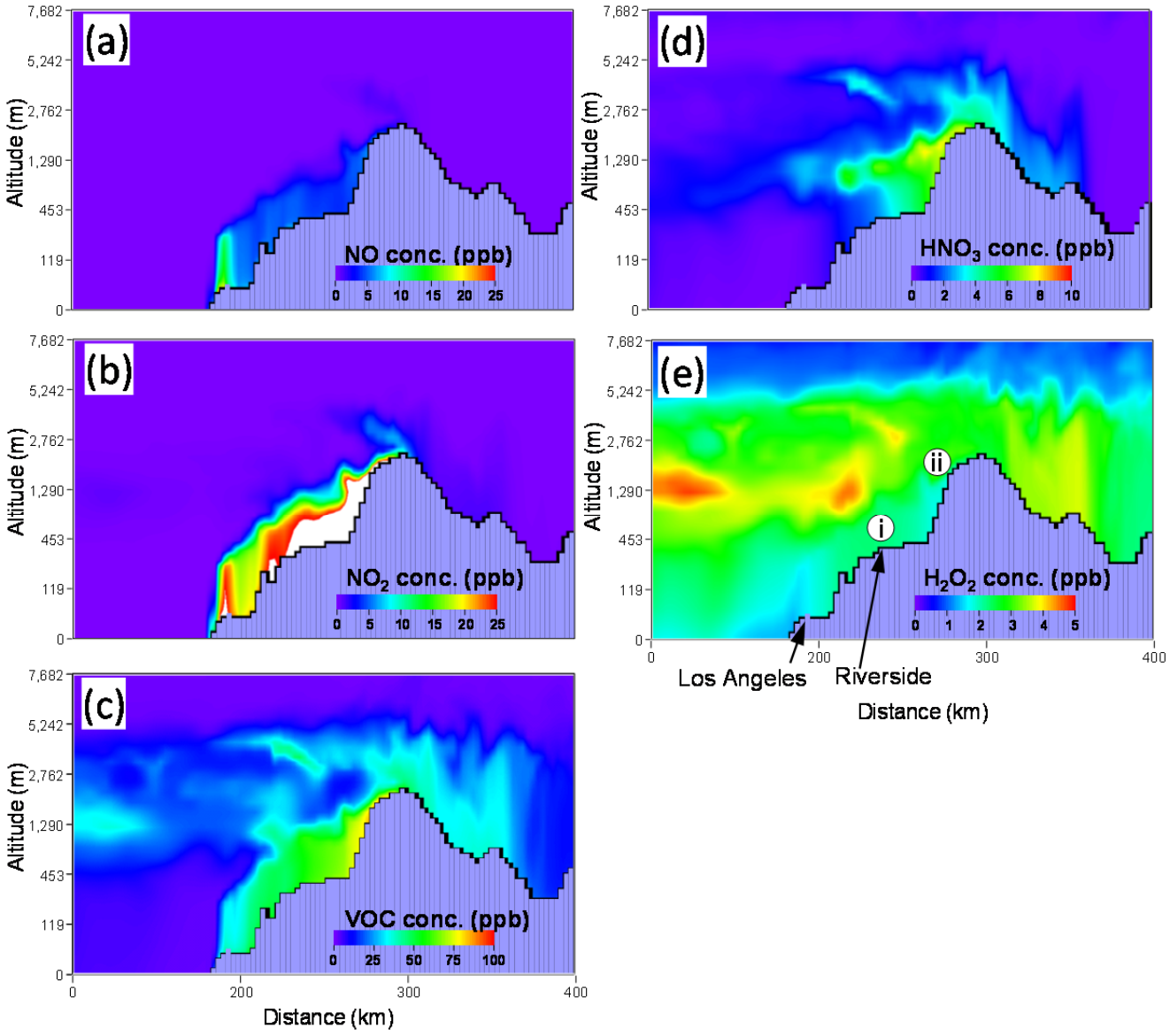

Fig. 3. Vertical cross-section of air pollutant concentrations near over the San Bernardino mountain range at 1800 PST on July 17, 2005 for: (a) nitric oxide (NO), (b) nitrogen dioxide (NO_2); NO_2 concentrations >25 ppb are shown in white, (c) volatile organic compounds (VOCs), (d) nitric acid (HNO_3), and (e) hydrogen peroxide (H_2O_2). Symbols in Fig. 3(e) corresponds the position shown in Fig. 4.

increasing tendency with time (in other words aging) after when HNO_3 concentration shows decreasing trend in early afternoon. Grossmann *et al.* (2003) reported diurnal variations of H_2O_2 and HNO_3 concentrations in Berlin, Germany, and observed typical diurnal trend of both species. Fig. 4 shows the diurnal variation of H_2O_2 and HNO_3 and H_2O_2/HNO_3 ratios at Riverside (Fig. 4(i)) and on the western mountain slopes (Fig. 4(ii)). The time difference of HNO_3 peak at the western mountain slope which locates in the downstream of 52 km distance from Riverside, showed 4 hours. However, H_2O_2/HNO_3 ratio increased almost same time at 1600 PST. The maximum H_2O_2/HNO_3 ratio near Riverside was 1.57, somewhat higher than the 0.5 ratio reported by Grossmann *et al.* (2003) in Berlin. This ratio increased to 5 at the San Bernardino Mountains during the night, and to ~10 in the morning, as HNO_3 concentrations decreased to nearly zero in the aged air mass. The H_2O_2/HNO_3 peaked near the mountain range summit.

The non-linear relationship between O_3 contributions and H_2O_2/HNO_3 ratios is examined in Fig. 5. In order to understand source contributions to O_3 concentrations and O_3 precursors, the Zero-Out method for the seven emission source categories was used. A rapid increase in the vehicle exhaust contribution to O_3 formation was found for H_2O_2/HNO_3 ratios from 0.1 to ~1.6. As air mass ages, vehicle contribution decreases with increasing H_2O_2/HNO_3 ratios from ~1.6 to ~3. Biogenic contributions to O_3 seem to be more sensitive to the H_2O_2/HNO_3 ratio with the highest contribution found at the lowest ratios. Figs. 5(a) and 5(b) show the results reflecting the impact of NO_x and VOC

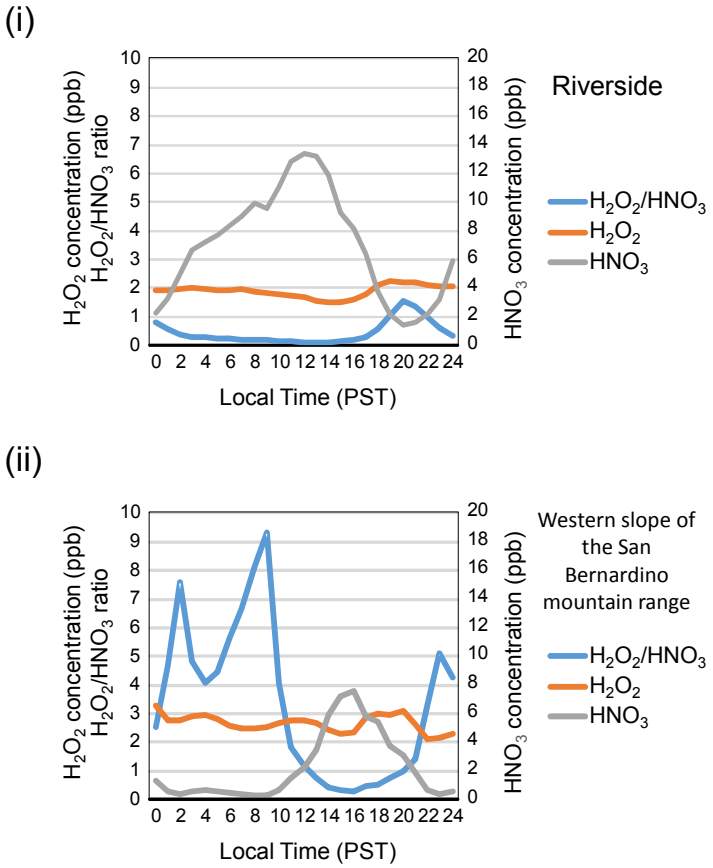

Fig. 4. Diurnal variation of H_2O_2 and HNO_3 and H_2O_2/HNO_3 ratios on July 17, 2005 for: (i) at Riverside and (ii) western slope of the San Bernardino mountain range.

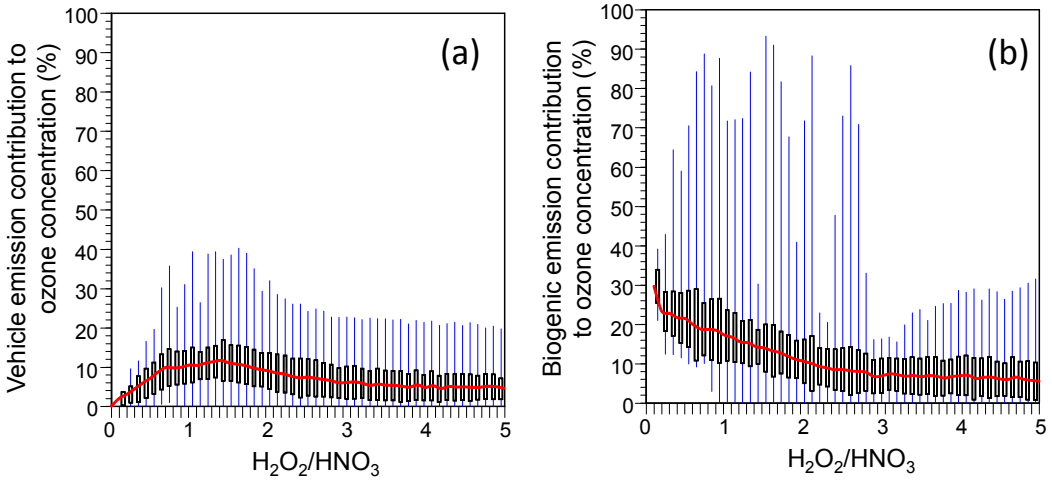

Fig. 5. Source contributions to O_3 concentrations as a function of H_2O_2/HNO_3 ratios for: (a) engine exhaust, and (b) biogenic emissions, obtained from the cross-sectional area shown in Figure 1b from 1300 to 2300 PST on July 17, 2005. The red line shows average source contributions. The box plot gives the standard deviation of source contributions. The blue line shows maximum and minimum values of source contributions.

emissions, respectively, and their distribution as a function of H_2O_2/HNO_3 ratio are consistent with the result of Silman (1995). Contributions to O_3 formation levels off for both sources as H_2O_2/HNO_3 ratios exceeded 3. However, the result of Silman showed lower value (0.3–0.5).

DISCUSSION

Fig. 6 shows average O_3 concentrations from 1300 to 2300 PST on July 17. A high O_3 concentration (hot spots) was often seen near top of PBL and vertical circulation

area promoted by the mountain chimney effect during the simulation period. These areas were the accumulation area of air pollutants after transportation of the updraft flow. Since the production mechanism of each hot spot is different, a base case O_3 concentration and emission source contributions at time of the localized O_3 maxima are shown in Fig. 6. The hot spot pollutant concentrations and H_2O_2/HNO_3 ratios are summarized in Table 3.

At 2100 PST on July 17, Location No. 1 (elevation ~990 m) in Fig. 6 represents transport from the northwest, with the highest H_2O_2 (4.9 ppb) and lowest HNO_3 (1.1 ppb) concentrations, characteristics of an aged air mass. Source contributions to O_3 were dominated by residential emissions, accounting for 36.5% of O_3, followed by biogenic sources (26.1%). On-road gasoline and diesel exhaust contributions were 4.8% and 4.1%, respectively.

The maximum O_3 concentration of 110 ppb was found at Location No. 2, situated ~990 m above an urban area between the cities of LA and Riverside at 1700 PST. In contrast to Location No.1, No. 2 showed the lowest level H_2O_2 (3.0 ppb) and highest HNO_3 (11.3 ppb) concentrations among the six points, characteristic of a fresh air mass. Biogenic

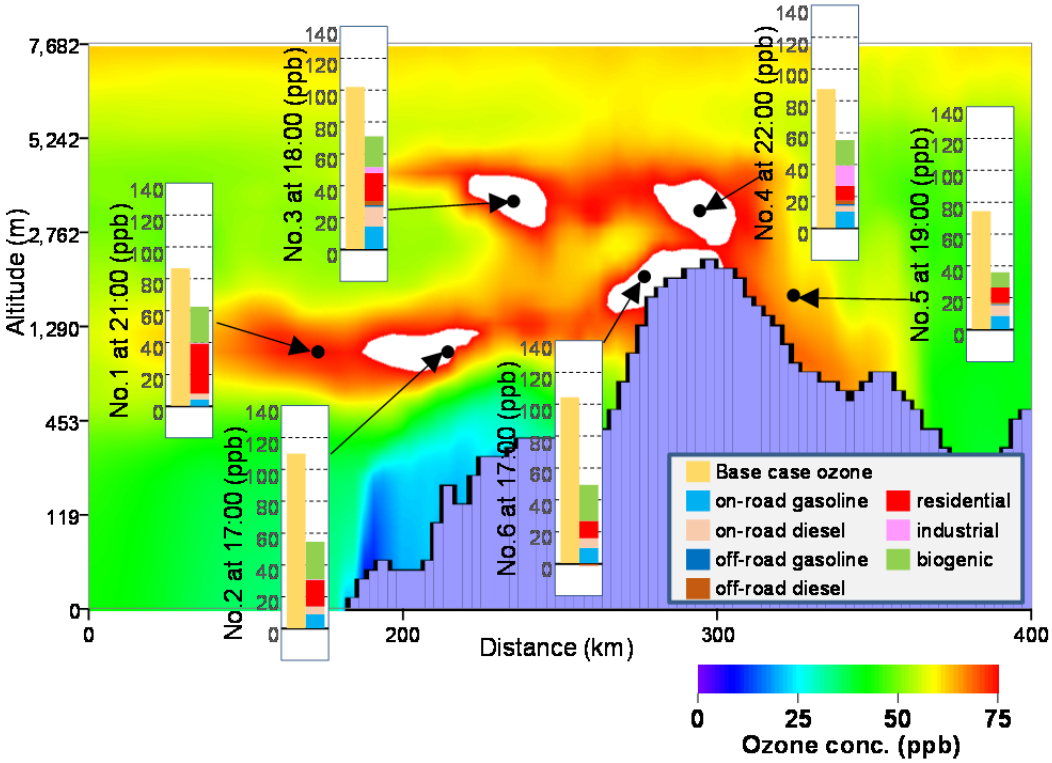

Fig. 6. Time averaged (1300 to 2300 PST on July 17, 2005) hot spots (O_3 > 75 ppb, indicated by black dots) with emission source contributions determined by the zero-out cases for: 1) largest residential emission contribution (36.5%); 2) largest biogenic emission contribution (21.6%); 3) largest on-road gasoline engine emission contribution (13.9%); 4) largest industrial emission contribution (14.6%); 5) lowest biogenic contribution (12.7%); and 6) largest VOC and NO_2 concentrations, and 2nd highest biogenic contribution (21.7%) to O_3.

Table 3. Hot spot pollutant concentrations and H_2O_2/HNO_3 ratios at different elevations from 1700 to 2200 PST on July 17, 2005.

Location	Map Location and Elevation	Time	Pollutant Concentrations (ppb)						H_2O_2/HNO_3
		PST	O_3	NO	NO_2	VOC	H_2O_2	HNO_3	
No. 1	Pacific Ocean (990 m)	2100	86.8	0.0	0.7	39.9	4.9	1.1	4.6
No. 2	Between Los Angeles and Riverside (990 m)	1700	110.1	0.4	3.5	41.1	3.0	11.3	0.3
No. 3	Northeast of Los Angeles (3417 m)	1800	102.2	0.0	0.3	48.0	3.8	3.5	1.1
No. 4	Above the summit of San Bernardino mountain range (3178 m)	2200	87.7	0.0	0.7	35.9	3.3	2.4	1.4
No. 5	East slope of San Bernardino mountain range (1650 m)	1900	74.6	0.0	0.6	33.0	3.4	1.9	1.8
No. 6	West slope of San Bernardino mountain range (1937 m)	1700	104.7	0.6	4.1	52.0	3.0	8.5	0.4

emissions constituted the highest source contribution, accounting for 21.6% of O_3, followed by residential emissions (15.1%) and engine exhaust (12.4%, mostly on-road gasoline emissions [7.9%]). The low H_2O_2/HNO_3 ratio of 0.3 suggests the atmosphere was VOC-limited for this part of the SoCAB. Residential and biogenic emissions contributed to 51.7 and 24.1% of total VOCs, respectively.

The highest engine exhaust contribution, accounting for 29.6% of O_3 (including 13.9% from on-road gasoline vehicle exhaust) was found at Location No.3 (elevation ~3417 m), over northeastern LA and Riverside, at 1800 PST. This was accompanied by a 19% contribution from biogenic and 17.5% from residential emissions. The second and third highest engine exhaust contributions were found at Locations No. 4 and No. 5 in Fig. 6, respectively, both of which are above the PBL and in the eastern part of the SoCAB. This suggests that engine exhaust emissions from the urban center began to oxidize, mix with biogenic emissions, and gradually contribute to O_3 formation during transport. The highest source contribution to O_3 at Location No. 4 was industry (14.6%). At Location No. 5, away from anthropogenic emission sources, the biogenic contribution to O_3 formation was the lowest (12.7%) among the hot spots. The highest VOC and NO_2 concentrations along with the second highest biogenic emission contribution (21.7%) to O_3 were found in Location No. 6, whereas the lowest VOC and NO_2 concentrations were found at the elevated Locations No. 4 and No. 5 toward the mountain and desert areas.

The mountain chimney effect is further demonstrated in Fig. 7 for the same time period (1300 to 2300 PST) on July 14. As seen in Fig. 6 for July 17, lower vehicle source contributions to O_3 were found at the lower elevation Locations No. 1 and No. 2 (elevation ~513–654 m), with higher exhaust contributions above the PBL at Location No. 3 (elevation ~2252 m) in Fig. 7. Elevated biogenic contributions were found both north of LA (Locations No. 2) and northwest of Riverside (Location No. 4) in Fig. 7.

CONCLUSIONS

This modeling study of O_3 near mountains in the eastern part of the South Coast Air Basin (SoCAB) identifies vertical wind velocity profiles with counter clockwise air flow on the west side of San Bernardino mountain range that enhances the up-slope mountain chimney effect with some circulation found on the east side. Elevated O_3 concentrations (> 75 ppb "hot spots") occurred near the top of the planetary boundary layer (PBL, ~1200 m), above the PBL over the city of Riverside, and at the free troposphere (~3500 m) in the eastern SoCAB. O_3 hot spots located near the urban areas between the cities of LA and Riverside show the highest HNO_3 and lowest H_2O_2 concentrations, suggesting O_3 formation in air masses with fresh vehicle emissions. Elevated O_3 concentrations over the Pacific Ocean with the highest H_2O_2 and lowest HNO_3 concentrations are consistent with transport of aged air parcels by the prevailing northwesterly winds down the coast from the Bay Area and/or Santa Barbara area. High O_3 concentrations above the PBL surrounding the mountain range indicate that O_3 from the basin is uplifted by vertical circulations. A rapid increase in vehicle exhaust contributions to O_3 formation was found at low (< 1.6) H_2O_2/HNO_3 ratios and leveled off as emissions age. Biogenic emission contributions to O_3 formation are more sensitive to the decreasing H_2O_2/HNO_3 ratios from 0.01 to 2.5. On-road engine exhaust contributions to O_3 are low (4.8%) above the Pacific Ocean, with the

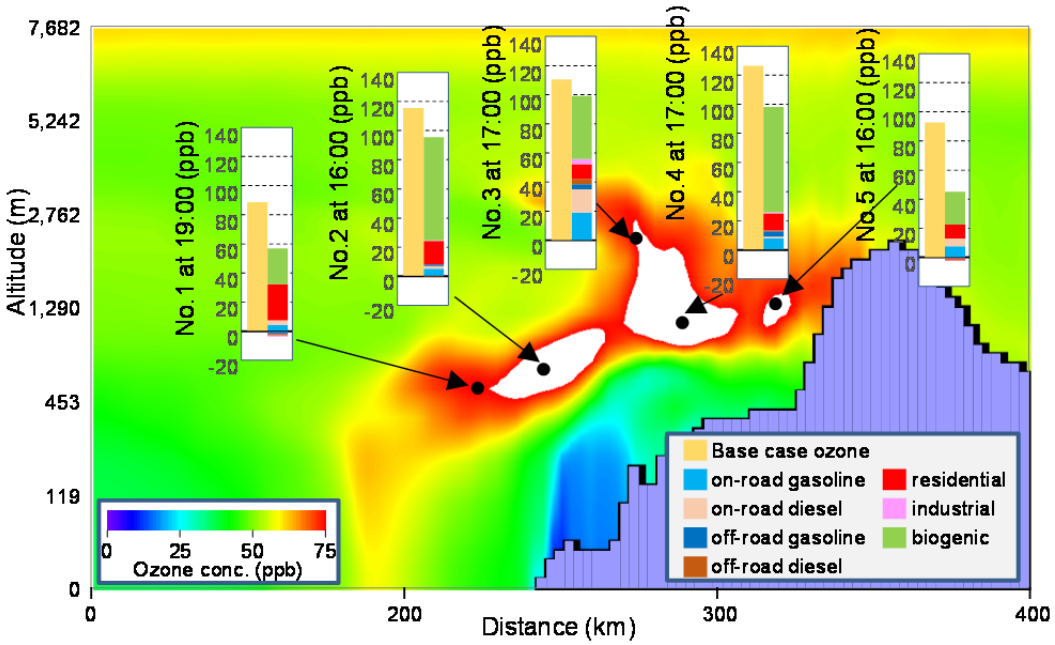

Fig. 7. Time averaged (1300 to 2300 PST on July 14, 2005) hot spots hot spots (O_3 > 75 ppb, indicated by black dots) with emission source contributions determined by the zero-out cases. (As hot spots were not found on the eastern side of the San Bernardino mountains, only the western side is shown.

highest contributions (13.9%) found above the PBL (~3417 m) outside of the LA urban areas. In contrast, the highest biogenic contribution (21.6%) was found near the urban area between the cities of LA and Riverside. These simulations emphasize the importance of understanding pollutant aging, evolution, and transport.

ACKNOWLEDGMENTS

This research was supported by the efforts of Darko Koracin, Amela Jericevic, Jinhua Jiang, and Travis Mccord of Desert Research Institute on input data creation. Simulations were conducted by the Newton High Performance Computing program, a joint effort among the Office of Research, the Office of Information Technology, and the Departments of the University of Tennessee. The authors thank Ms. Jo Gerrard of the Desert Research Institute for her assistance in preparing and editing the manuscript.

REFERENCES

Angevine, W.M., Eddington, L., Durkee, K., Fairall, C., Bianco, L. and Brioude, J. (2012). Meteorological model evaluation for CalNex 2010. *Mon. Weather Rev.* 140: 3885–3906.

Angevine, W.M., Brioude, J., McKeen, S., Holloway, J.S., Lerner, B.M., Goldstein, A.H., Guha, A., Andrews, A., Nowak, J.B., Evan, S., Fischer, M.L., Gilman, J.B. and Bon, D. (2013). Pollutant transport among California regions. *J. Geophys. Res.* 118: 6750–6763.

Byun, D. and Schere, K.L. (2006). Review of the governing equations, computational algorithms, and other components of the Models-3 Community Multiscale Air Quality (CMAQ) modeling system. *Appl. Mech. Rev.* 59: 51–77.

Collet, S., Kidokoro, T., Sonoda, Y., Lohman, K., Karamchandani, P., Chen, S. and Minoura, H. (2012). Air quality impacts of motor vehicle emissions in the south coast air basin: Current versus more stringent control scenario. *Atmos. Environ.* 47: 236–240.

Dunker, A.M. (1984). The decoupled direct method for calculating sensitivity coefficients in chemical kinetics. *J. Chem. Phys.* 81: 2385–2393.

Fujita E.M., Campbell D.E., Stockwell W.R. and Lawson D.R. (2013). Past and future ozone trends in California's South Coast Air Basin: Reconciliation of ambient measurements with past and projected emission inventories. *J. Air Waste Manage. Assoc.* 63: 54–69.

Grossmann D., Moortgat, G.K., Kibler, M., Schlomski, S., Bächmann, K., Alicke, B., Geyer, A., Platt, U., Hammer, M.U., Vogel, B., Michelcic, D., Hofzumahaus, A., Holland, F. and Volz-Thomas, A. (2003). Hydrogen peroxide, organic peroxides, carbonyl compounds, and organic acids measured at Pabstthum during BERLIOZ. *J. Geophys. Res.* 108: 8250.

Haagen-Smit, A.J. (1952). Chemistry and physiology of Los Angeles smog. *Ind. Eng. Chem.* 44: 1342–1346.

Janjic, Z., Gall, R. and Pyle, M. (2010). Scientific Documentation for the NMM Solver, NCAR Technical Note, NCAR/TN- 477+STR

Kato, T. and Saito, K. (1995). Hydrostatic and non-hydrostatic simulations of moist convection: Applicability of the hydrostatic approximation to a high-resolution model. *J. Meteorolog. Soc. Jpn.* 73: 59–77.

Langford, A.O., Senff, C.J., Alvarez, R.J., Banta, R.M. and Hardesty, R.M. (2010). Long-range transport of ozone from the Los Angeles Basin: A case study. *Geophys. Res. Lett.* 37: L06807.

Lu, R. and Turco, R.P. (1996). Ozone Distributions over the Los Angeles Basin: Three-dimensional simulations with the smog model. *Atmos. Environ*. 30: 4155–4176.

Sillman, S. (1995). The use of NO_y, H_2O_2, and HNO_3 as indicators for ozone-NO_x-hydrocarbon sensitivity in urban locations. *J. Geophys. Res.* 100: 14175–14188.

Sillman, S. and He, D. (2002). Some theoretical results concerning O_3-NO_x-VOC chemistry and NO_x-VOC indicators. *J. Geophys. Res.* 107: 4659.

Tonnesen, G.S. and Dennis, R.L. (2000a). Analysis of radical propagation efficiency to assess ozone sensitivity to hydrocarbons and NO_x 1. Local indicators of instantaneous odd oxygen production sensitivity. *J. Geophys. Res.* 105: 9213–9225.

Tonnesen, G.S. and Dennis, R.L. (2000b). Analysis of radical propagation efficiency to assess ozone sensitivity to hydrocarbons and NO_x 2. Long-lived species as indicators of ozone concentration sensitivity. *J. Geophys. Res.* 105: 9227–9241.

US.EPA (2007). Guidance on the Use of Models and Other Analyses for Demonstrating Attainment of Air Quality Goals for Ozone, $PM_{2.5}$, and Regional Haze, Report USA EPA-454/B-07-002, U.S. Environ. Protect. Agency, Washington, DC.

Yarwood, G., Wilson, G., Morris, R.E., and Yocke, M.A. (1997). *User's Guide to the Ozone Tool: Ozone Source Apportionment Technology for UAM-IV*, Report prepared for the South Coast Air Quality Management District, Diamond Bar, California.

Zhang, Y., Wang, W. Wu, S. Wang, K. Minoura, H. and Wang, Z. (2014). Impacts of updated emission inventories on source apportionment of fine particle and ozone over the southeastern U.S. *Atmos. Environ.* 88: 133–154.

Received for review, September 18, 2015
Revised, February 25, 2016
Accepted, February 28, 2016